Pulsed Star Labeling of Arterial Regions (PULSAR): A Robust Regional Perfusion Technique for High Field Imaging

Xavier Golay,* Esben T. Petersen, and Francis Hui

Regional perfusion imaging (RPI) has recently been introduced as a potentially powerful technique to map the perfusion territories of patients with vascular diseases in a fully noninvasive manner. However, this technique suffers from the problems of the transfer insensitive labeling technique upon which it is based. In particular, RPI is very sensitive to magnetic field inhomogeneities, and therefore the definition of the labeled bolus can deteriorate at field strength higher than 1.5 T. Furthermore, the slab-selective triple-pulse postsaturation sequence used originally will also be impaired due to the same problem, rendering RPI unusable at higher field. In this work, an adiabatic-based signal targeting with alternating radiofrequency pulses sequence is proposed as a labeling scheme to solve the problems related to variations in local magnetic field, together with an improved four-pulse water suppression enhanced through T_1 effects technique as a presaturation scheme. Magn Reson Med 53: 15–21, 2005. © 2004 Wiley-Liss, Inc.

Key words: arterial spin labeling; regional perfusion imaging; 3.0 T; magnetic field inhomogeneity insensitive technique

Recently, several methods have been introduced for noninvasive regional perfusion imaging (RPI) of individual perfusion territories (1–5). These RPI methods bear the promise of providing vascular–anatomic information and therefore rendering the assessment of collateral flow possible in a complete noninvasive manner. When combined with other MRI techniques, such as diffusion-weighted imaging (DWI), these methods are foreseen as of potentially great clinical value for the early diagnosis of neurovascular diseases like arteriosclerosis or focal cerebral ischemia.

However, thus far only a few reports have been published on techniques capable of providing robust quantifiable multislice RPI. Edelman et al. were the first to introduce the use of selective presaturation of individual arteries for the angiographic examination of the circle of Willis in patients with cerebrovascular diseases (6). However, no perfusion was measured in this work. Using continuous arterial spin labeling techniques, several groups have proposed the use of individual surface coils to selectively label the left or right common artery individually (1,2,7,8). Although they are perfectly quantifiable, these methods suffer from the small penetration power of the local sur-

face coils, rendering them unusable for the independent labeling of the posterior circulation.

Recently, a few groups have come up with potential pulsed ASL techniques for the selective tagging of individual arteries, using either sagittal (3) and anatomy-driven (4) angulated spatially selective slabs or two-dimensional labeling pulses forming a pencil beam profile (5). The method used by Hendrikse et al. (4) is interesting as quantitative perfusion values can be obtained using the model of Calamante et al. (9). This RPI technique was based on the transfer insensitive labeling technique (TILT) (10), a magnetization-transfer insensitive technique using two concatenated Shinnar–Leroux optimized sinc-gauss pulses to achieve either a $90 + 90° = 180°$ or $90 - 90° = 0°$, depending on the phase of the second pulse (11). This way of concatenating pulses has the advantage, but also the inconvenience of exactly doubling the flip angle of the pulse at any place in the labeled slab (11). In fact, the improved definition of the inversion slab due to this effect becomes a major limiting factor in inversion efficiency when the magnetic field homogeneity degrades.

In order to increase perfusion sensitivity, high field imaging is appealing because it combines the advantages of higher intrinsic signal-to-noise ratio (SNR) with increased relaxation time (T_1) of the labeled blood (12). The major drawback of high field imaging resides in the reduced RF penetration and increased RF power deposition. The latter will induce larger variations in the applied radiofrequency field (B_1), rendering the TILT labeling particularly inefficient if the individual pulses can't achieve a proper saturation. For similar reasons, the triple pulse CHESS-like (chemical shift selective) (13) presaturation sequence can be suboptimal to avoid contamination of the labeling slab in the measured perfusion areas if nonadiabatic pulses are used.

To avoid effects of both ineffective labeling and artifactual direct tagging of the tissue of interest, we propose in this work to use a multislice EPISTAR-based technique for labeling (14) combined with an optimized water suppression enhanced through T_1 effects (WET) technique for proper presaturation of the imaging volume (15), as opposed to the postsaturation used in the original RPI sequence. This new technique is dubbed PULSAR, for pulsed STAR labeling of arterial regions. The higher intrinsic SNR, combined with the longer blood T_1 relaxation time, allows us for the first time to achieve complete supratentorial regional perfusion imaging in a scan time of 3–5 min per region.

MATERIALS AND METHODS

STAR Labeling Sequence

A conventional multislice signal targeting by alternating radiofrequency pulses (STAR) sequence was chosen for
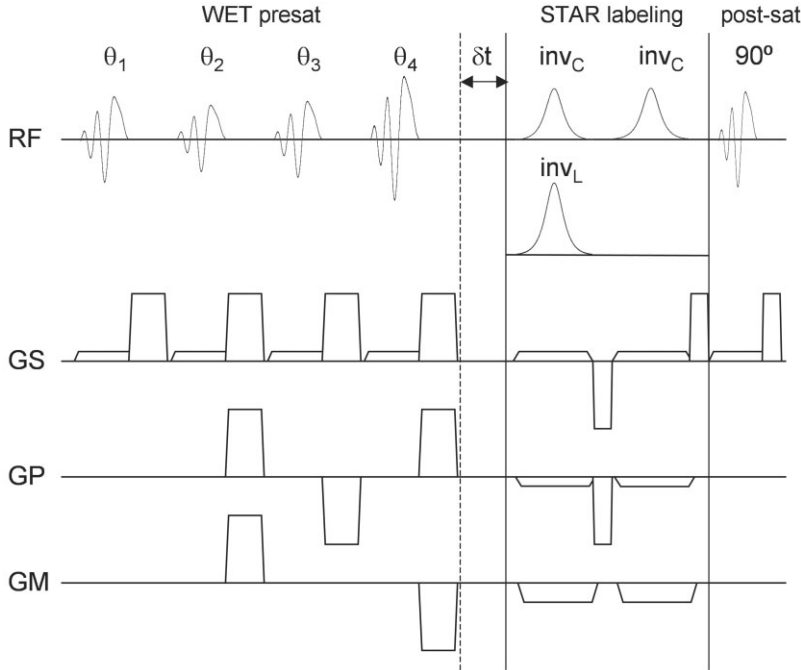
FIG. 1. PULSAR labeling and control sequences. The sequence is composed of three parts. In the first, an optimized four-pulse WET presaturation sequence is applied with $\theta_1 = 88.9°$, $\theta_2 = 98.7°$, $\theta_3 = 82.5°$, and $\theta_4 = 159.0°$. This saturation slab is parallel to the volume of interest and usually extends both proximally and distally by a few centimeters. A gradient cycling is performed to avoid stimulated echoes. Then a STAR labeling sequence is performed with either a single 13.3-msec hypersecant AFP pulse (inv_L) with BW = 1.2 kHz and $B_1 = 13.5$ μT for labeling or two AFP pulses of identical length and BW and $B_1 = 9.55$ μT for the control acquisition (inv_C). Note that the angulations of this STAR sequence can be arbitrary with respect to the volume of interest. Finally, a 90° dephasing pulse is applied with the same geometry as during the presaturation sequence to provide a clear starting time of the bolus. This sequence will normally be followed after typical delay time of 1.5 sec by a multislice, single-shot EPI readout (not shown).

labeling (14). In this sequence, both control and labeling pulses are performed at the same location, while the RF power of the first (labeling) 180° inversion pulse is counterbalanced using two consecutive adiabatic pulses of half RF power during the control phase, resulting in a net 180 + 180° = 0° pulse in the nonlabeled case. The associated induced magnetization transfer effects are identical in both cases, which allows multislice and 3D perfusion imaging and, in our case, independent positioning of the labeling pulses with respect to the slices of interest. The adiabatic pulses used in the present implementation are conventional hypersecant pulses, but more specialized pulses such as FOCI pulses (16) can also be used instead. The labeling sequence is preceded with a WET pre-saturation scheme and followed by a single 90°-dephasing pulse to ensure identical timing between both labeling and control experiments (see Fig. 1).

WET Presaturation Pulses

The four-pulse saturation sequence used in this work is adapted from the WET saturation scheme originally used for spectroscopy (15). In this paper, the authors demonstrated that this four-pulse scheme achieves a better water suppression than conventional three-pulse CHESS saturation schemes over a wide range of T_1 values and B_1 inhomogeneities (13). When optimizing PULSAR for MR perfusion imaging at 3.0 T, the pulse duration of the presaturation sequence and therefore the time τ between successive pulses can be considerably shorter than the spectrally selective (50−60 Hz) water suppression pulses used for spectroscopy. In particular, we used numerically optimized saturation pulses capable of providing sharp profiles while remaining relatively short to maximize their bandwidth, which is desirable in such a case to avoid bending of the presaturation slab.

In order to get optimal water saturation over a wide range of B_1 fields, a series of numerical simulations of the WET sequence were performed using the following description for the residual magnetization M_R to be minimized under large B_1 and T_1 ranges,

$$M_R(n) = M_0\{(1 - e^{-TR/T_1})e^{-n\tau/T_1} \cos\theta_1 \cos\theta_2 \ldots \cos\theta_n$$
$$+ (1 - e^{-\tau/T_1})[e^{-(n-1)\tau/T_1} \cos\theta_2 \cos\theta_3 \ldots \cos\theta_n$$
$$+ \ldots + e^{-\tau/T_1} \cos\theta_n + 1]\}, \quad [1]$$

where M_0 is the equilibrium magnetization, n is the number of applied suppression pulses, θi is the flip angle of the ith RF pulse, and TR is the overall repetition time. This approximation of the residual magnetization assumes complete dephasing of the spins in between pulses and localized instantaneous RF pulses.

The optimization was written on IDL 6.0 (Research Systems, Inc., Boulder, CO) using a multidimensional minimization routine (AMOEBA) based on the downhill simplex method of Nelder and Mead (17). To ensure proper reaching of a global minimum, a sweep through all starting flip angles from 0 to 180°in steps of 3° for each of the four pulses was performed. The algorithm was constrained to exclude suboptimal solutions with flip angles larger than 180°.

In the original WET paper, the authors showed that smaller values of τ improve the saturation. Therefore, in the present optimization, we chose the shortest time possible ($\tau = 10$ msec) to accommodate the RF pulse, spoiling gradients, and eddy-current decay period on our system.

An appropriate range of T_1 values has to be selected for brain tissue at 3.0 T. We used accurate T_1 maps recently acquired by Lu et al. ($n = 8$) at this field strength (Lu et al., private communication). The cumulative distribution of

all T_1 values over the eight volunteers demonstrated that 99% of the total amount of pixels had T_1 values in the range $400 \leq T_1 \leq 4200$ msec, which was therefore chosen for optimization. This T_1 range was obtained on normal volunteers, but should still be valid for pathologic tissue, as T_1 tends to shift toward higher values in this case and will therefore remain inside the optimized range (18).

The B_1 field variations are more difficult to estimate or measure, as they depend on the coil loading factor and the size of the volume of interest. Here we optimized the saturation by assuming B_1 homogeneity to stay within $\pm 10\%$ of the nominal B_1 value, as we were using the body coil for transmitting. We compared the simulated four-pulse WET scheme to numerical simulations of the original RPI approach (4), which used three 90° pulses after labeling.

Finally, in order to account for the finite duration of the RF pulses, the potential incomplete dephasing of the magnetization in between RF pulses and the actual B_1 distribution, an additional calibration step has to be done to adjust the "zero-level" of the signal after the last WET pulse. This calibration was done both on phantoms and on humans by changing the last flip angle or the delay time from the last saturation pulse to the inversion pulse (15).

MR Experiments

All experiments were performed on a 3.0-T Philips Intera Imager (Philips Medical Systems, Best, The Netherlands) equipped with Master gradients (30 mT/m strength and 120 mT/m/msec slew rate). All images were acquired using the quadrature body coil as sending coil for optimal B_1 homogenity and a dedicated eight-element phased-array head coil (MRI Devices Corp., Waukesha, WI) as receiving coil.

Prior to human scanning, phantom measurements were performed to verify and quantify the obtainable signal suppression obtained by the WET presaturation pulses. All phantom experiments used the following parameters: slice thickness = 15 mm; matrix = 128 × 128; FOV = 240 mm; TR/TI/TE/α = 3000 msec/10 and 260 msec/ 15 msec/90°; multishot EPI; EPI factor 5; 10 averages; inversion slab width = 30 or 50 mm.

Two tests were carried out. First a single phantom with a T_1 of 400 msec was placed in the scanner, and both WET presaturation sequence and STAR labeling slabs were placed perpendicular to the imaging slice and to each other. This provided the full signal (M_0), the saturated signal where image slice and inversion plane intersect ($M_{R,int}$), and the saturated signal for the image slice only ($M_{R,img}$) in a single acquisition. The degree of saturation was measured as ($M_{R,i}/M_0$) × 100%.

In a second experiment, a 50-mm inversion slab was placed through five phantoms, each having different T_1 values to ensure that the saturation works equally well over a wide T_1 range. The experiment was repeated without saturation pulses in order to get the nonsaturated signal intensity. T_1 values of 160, 400, 900, 1700, and 2500 msec were obtained using organic oil, 0.08% $CuSO_4 \cdot 5H_2O$, 1.2% agar + 0.08% ferrous fumerate ($C_4H_2O^4Fe$), 2.4% agar + 0.04% ferrous fumerate, as well as physiologic saline solution, respectively.

Four volunteers gave written informed consent before participation. This study was run under a general protocol for pulse-sequence development approved by the local ethics committee.

For each volunteer, after a conventional MR localizer followed by a SENSE reference scan, a fast (2-min) 3D time of flight (TOF) MRA measurement was performed to visualize the circle of Willis with subsequent three-plane maximum-intensity projection (MIP) reconstructions. The scan parameters were TR/TE = 16.2/2.7 msec; flip angle = 20°; field of view = 220 × 188 mm; matrix size = 352 × 224; slice thickness = 1.5 mm (reconstructed = 0.75 mm); number of slices = 168; SENSE factor = 3.

Planning of the labeling volume was performed on the basis of three MIPs of the TOF MR angiogram in a way similar to that of Hendrikse et al. (4). In short, the size of the labeling slab can be adjusted in one direction and is infinite in the other two directions. For the selective labeling of ICAs, an oblique sagittal labeling slab was chosen based on the axial and coronal MIPs of the circle of Willis. The slab was aligned such that each ICA was labeled independently and signal contribution from the contralateral ICA, as well as the basilar and vertebral arteries, was avoided by lateral angulation of the posterior and proximal part of the labeling slab. For the selective labeling of the posterior circulation, both axial and sagittal MIPs of the circle of Willis were used, together with the native TOF images for verification of the minimal amount of contamination by the posterior labeling to both ICAs (see Fig. 3a), not always completely avoidable.

Regional perfusion imaging was then performed on all volunteers using the following parameters: TR/TI/TE/α = 3000 msec/1500 msec/9.2 msec/90°; single-shot EPI; SENSE factor 3; 50 pairs of labeled–control; FOV = 240 mm; 13 slices; matrix = 64 × 64 or 80 × 80 (reconstructed as 128 × 128); slice thickness = 6 mm; scan time = 3 perfusion territories × 3 to 5 min = 9 to 15 min. Longer scan times were used at higher in-plane resolution to compensate for the lower expected SNR.

Postprocessing

All images were exported on a Windows PC running IDL 6.0. No motion correction was performed. Instead, pairs of images showing strong motion artifacts were discarded prior to averaging according to the method described in Ref. (19). The raw images were then modulus subtracted to produce perfusion maps according to the equation (9)

$$\text{CBF} = \left(\frac{2\alpha_0}{\lambda} \frac{M_0}{\Delta M} \left(\frac{e^{-\text{TI} \cdot R_{1\,\text{app}}} - e^{-\text{TI} \cdot R_{1b}}}{R_{1b} - R_{1\,\text{app}}} \right) \right)^{-1}, \qquad [2]$$

where α_0 = labeling efficiency = 1, λ = blood brain partition coefficient = 0.9 mL/g, $R_{1\text{app}}$ = apparent longitudinal relaxation rate of the tissue = $1/T_{1\text{app}}$ = 0.91 sec^{-1} (corresponding to $T_{1\text{app}}$ = 1.1 sec) and R_{1b} = blood longitudinal relaxation rate = $1/T_{1b}$ = 0.59 sec^{-1} (corresponding to T_{1b} = 1.68 sec (12)).

Finally, all three perfusion maps (in ml/min/100 g) were combined into a red–green–blue (RGB) frame, without thresholding of any kind, in order to demonstrate the good spatial coherence of the perfusion territories reached with

this method. In Fig. 3b in particular, the left ICA is in green, the right ICA in red, and the posterior circulation in blue. Any area demonstrating mixing of perfusion coming from more than one vessel will show a combined color, e.g., perfusion coming from both ICA will turn yellow = red + green.

RESULTS AND DISCUSSION

WET Presaturation Pulses

The AMOEBA algorithm was robust in the minimization of M_R and the same global minimum was reached, regardless of the initial guess. Simulated maximum errors (M_R/M_0) × 100% at different delay intervals τ = 5.3, 10, 20, and 40 msec were 0.081, 0.085, 0.10, and 0.19%, respectively. This is in agreement with the results from Ogg et al. (15), stating that by decreasing τ the maximum saturation error will also be reduced as well. Therefore, the shortest practically feasible τ of 10 msec was used. When optimizing for $400 \leq T_1 \leq 4200$ msec and $\Delta B_1 = \pm 10\%$, the following flip angles were obtained: θ_1 = 88.9°, θ_2 = 98.7°, θ_3 = 82.5°, and θ_4 = 159.0°. Figure 2a shows the T_1 dependence at nominal B_1 using these flip angles (solid) and 3 times 90°(dotted). The B_1 dependence in Fig. 2b was simulated at a T_1 of 920 msec, which was the peak of the T_1 histograms. From these simulations it is clear that the triple-pulse CHESS saturation scheme does not perform as well as the four-pulse WET presaturation, demonstrating much higher sensitivities to ΔB_1 and ΔT_1 values. The 3D plot in Fig. 2c shows the maximum error as a function of T_1 and B_1 variation.

In order to get the best possible saturation, ad hoc calibration of the sequence is needed. The best way to accomplish this calibration is to add a small delay time at the end of the WET sequence. The need for calibration is due to the fact that the simulations are based on simplified signal equations, where complete dephasing of the spins in between pulses and localized instantaneous RF pulses are assumed. Furthermore, the actual B_1 in a region of interest may differ from average nonlocalized system B_1 estimation, and this would affect the center of the expected coil B_1 distribution. By extending the delay time by 20 msec the best saturation was achieved having ($M_{R,int}/M_0$) × 100% = 2.1% and ($M_{R,ima}/M_0$) × 100% = 2.3% at the intersection of the imaged slice and the labeling plane and solely in the imaged slice, respectively. The saturation efficiency does not match the simulated values of around 0.1%, but care should be taken in interpreting these results as, e.g., the Rayleigh noise distribution near zero plays an important role in this case. Furthermore, the difference between the two areas in the subtracted images is of greater importance. This difference $\Delta M_{R,int}/M_0$ was 0.3% and $\Delta M_{R,img}/M_0$ 0.07% for both areas, respectively (after a T_I = 10 msec), and needs to be compared to an expected $\Delta M/M_0$ of ~1% due to perfusion only.

This calibration was carried out in a volunteer as well, and the optimum additional delay time δt between the WET and STAR sequences was found to be around 20 msec as well. This test should be carried out once when implementing the sequence in the first place or after major hardware changes. In our experience, no readjustment was necessary before RPI scanning of individual volunteers.
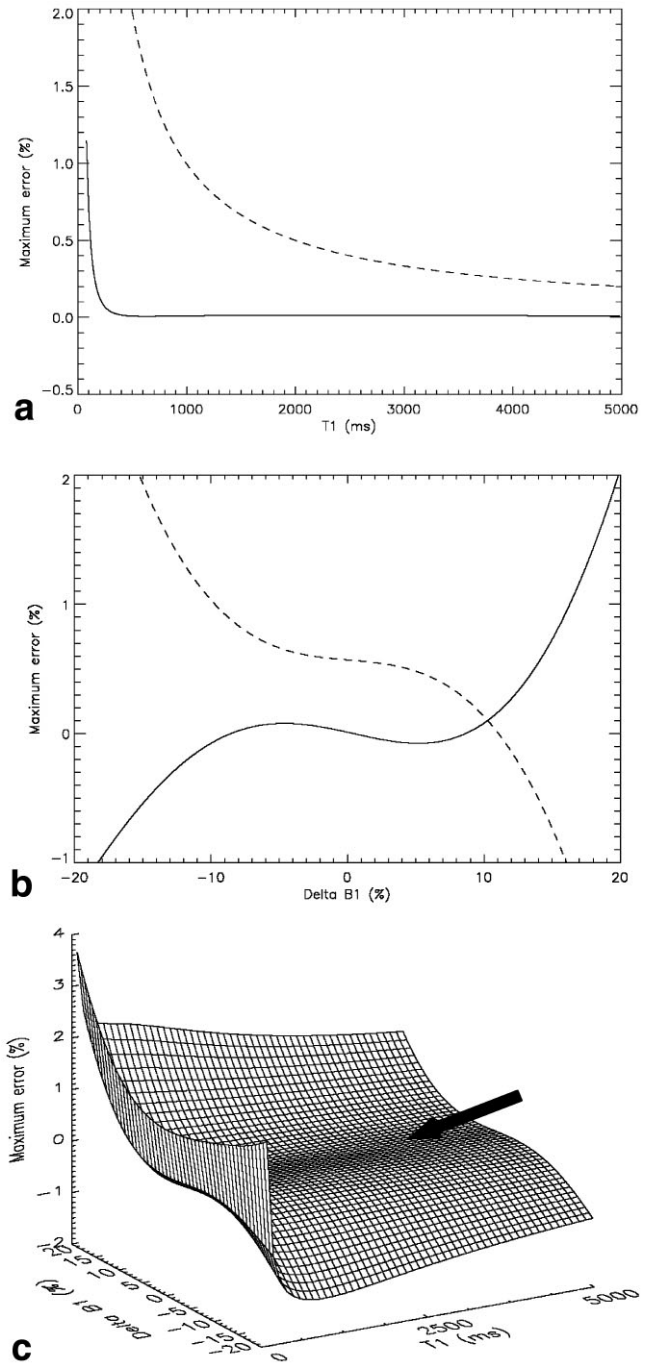
FIG. 2. Residual water magnetization MR after presaturation. (**a**) M_R as a function of T_1 for the WET presaturation sequence with θ_1 = 88.9°, θ_2 = 98.7°, θ_3 = 82.5°, and θ_4 = 159.0° (plain line) and after a triple 90° dephasing pulse sequence (dotted line). Note the very efficient saturation of the WET sequence in this case over a wide range of T_1 values. (**b**) Effects of the variation in the B_1 field on the remaining magnetization. Note the small remaining signal after the WET pulse within the ±10° range (plain line) compared to the triple 90° dephasing sequence. (**c**) Surface plot of the optimized WET sequence in the B_1–T_1 plane, demonstrating the large plateau area (arrow) for which M_R will stay theoretically minimal.

Table 1

Remaining Magnetization M_R after WET Presaturation Pulses Inside and Outside of the Labeled Volume (after T_1 = 10 msec), as well as Difference between Control and Tag as a Function of T_1

Phantom	$(M_R/M_0) \times 100\%$				$(\Delta M_R/M_0) \times 100\%$	
	Inside labeling slab		Outside labeling slab		Inside labeling slab	Outside labeling slab
T_1 (msec)	Tag	Control	Tag	Control	Control-tag	
160	1.43	1.29	2.33	2.72	0.25	0.09
400	0.94	1.05	2.32	2.18	0.31	0.02
900	0.61	0.66	0.61	0.61	0.09	−0.01
1700	0.31	0.12	0.42	0.41	0.05	0.05
2500	0.14	0.14	0.29	0.30	0.00	0.00

The capability of saturating at different T_1 values was tested using five different phantoms. The results are summarized in Table 1. The saturation efficiency decreases when going toward lower T_1 values, as expected according to Fig. 2c. The results indicate that T_1 values within the range 400 [lteq] T_1 [lteq] 4200 are saturated to a degree usable for arterial spin labeling as the subtracted signal (Control–Tag)

inside and outside the inversion slab do not exceed ~10% of the expected signal changes due to perfusion.

Regional Perfusion Images

Figure 3 describes typical RGB-encoded perfusion territories in a healthy volunteer. This color coding is very useful
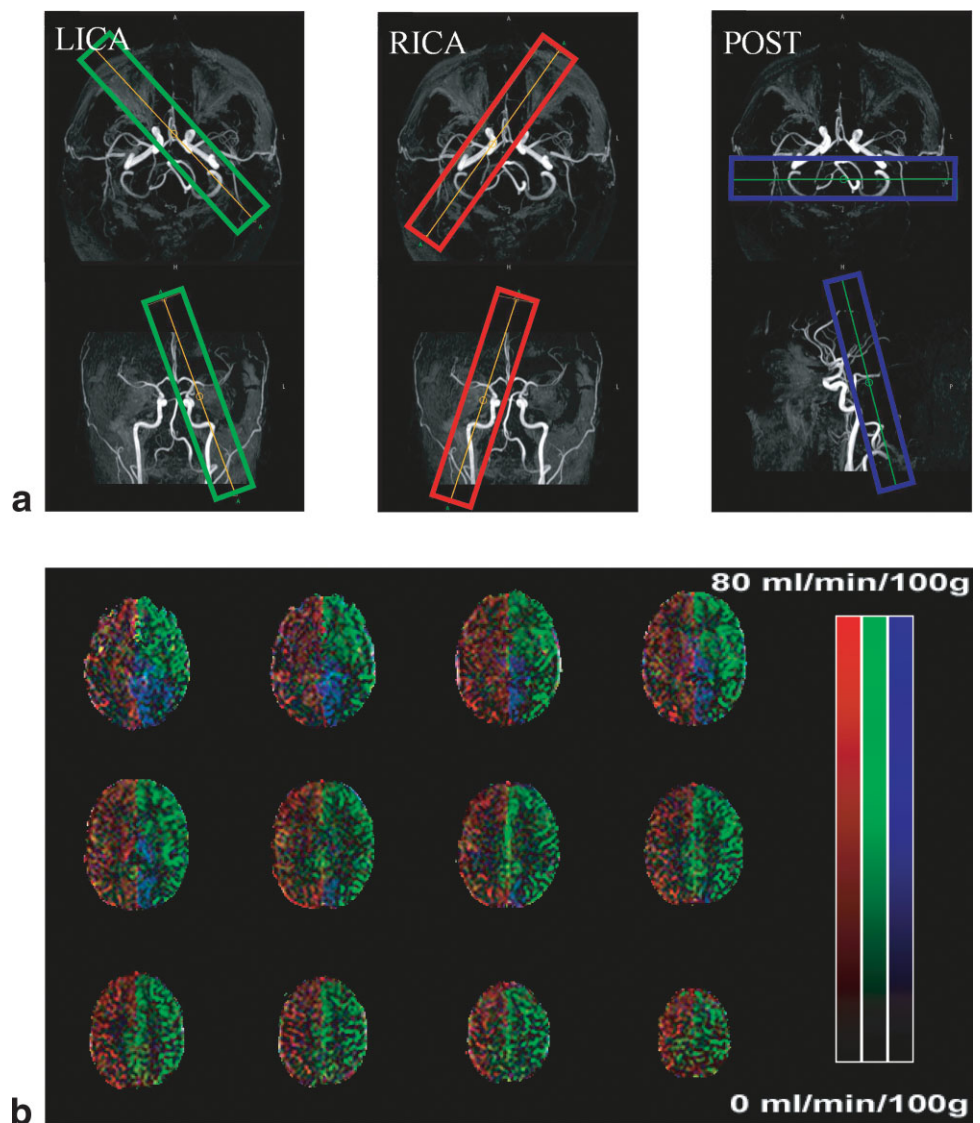

FIG. 3. (**a**) Planning of the respective labeling of the left ICA (green), right ICA (red), and posterior circulation (blue) on the MIPs of the circle of Willis of a healthy volunteer. See text for planning instructions. (**b**) Corresponding RPI image of all three perfusion territories of this volunteer.

for the assessment of each individual perfusion territory and, in pathologic cases, would allow the measurement of the mixing of blood coming from various territories via collaterals (in case of reduced blood through one of the major ICAs, for example).

In all volunteers, and to avoid appearance of a labeled sagittal sinus, the presaturation slab was extended distally to the volume of interest by 2–5 cm, depending on the angulation. Furthermore, in order to achieve a proper presaturation at the base of the volume of interest, the presaturation was also extended proximally by 2 cm. No significant signal inversion remaining in the perfusion maps could be seen in any volunteer.

One inherent problem of the method resides in the fact that it is largely restricted to supratentorial coverage. In fact, labeling of the cerebellum would be in most cases anatomically impossible. In some patients, however, and if really needed, an oblique coronal acquisition can be performed with a careful planning, trying to avoid saturating the basilar and vertebral arteries. Generally, the obtainable coverage at 3.0 T is much more important that what can be achieved at 1.5 T, at which field strength only five slices were acquired so far (4).

Figure 3 shows the perfusion territories from all three major arteries (left ICA, right ICA, and basilar artery). Note that in this case, the volunteer presented with two variations in the circle of Willis: First, there is a fetal right posterior communicating artery, leading to the fact that the right ICA delivers blood to the entire hemisphere and the posterior circulation only to the left posterior territory. Furthermore, although presenting with an otherwise normal circle of Willis, the right middle cerebral perfusion territory of this volunteer is supplied by the left side, as demonstrated by the invading green-labeled perfusion in the upper six slices.

The use of the second STAR version as labeling scheme allows achieving a highly effective labeling of each individual major artery separately. No reliable and reproducible result could be obtained using TILT (data not shown). In the present implementation, relatively long (13.3 msec) adiabatic full passage (AFP) pulses were used for labeling, in order to keep the adiabaticity with a reduced maximum B_1 in the control case. In fact, a reduction of B_1 by $\sqrt{2}$ in the control experiment was necessary in order to keep the power deposition of both labeling and control sequences identical, in a fashion similar to the one proposed by Alsop and Detre for single-coil continuous ASL (20). These long AFP pulses have the drawback of requiring more energy deposition, especially using the quadrature body coil as sending coil. However, SAR limits were never even closely reached in this study (max SAR = 0.3), due to the relatively low RF duty cycle of the sequence.

But the main problem resides in the absolute quantification of the perfusion. First of all, in this paper, a simple equation was chosen for estimation of the CBF value, using an averaged T_{1app} of 1100 msec for the entire brain, which can lead to some errors in the white matter CBF (9). Furthermore, this unique value was also used to estimate M_0. Then, by alternatively labeling each major artery separately, and depending on the geometry, the length of the labeled bolus as well as its time of arrival will be different for each perfusion territory, which can lead to errors in the

quantification, if one considers the general kinetic model for PASL sequences (21). This effect can become particularly important when comparing the perfusion signal in the more distal slices, coming from both ICAs to that of the posterior circulation, directly supplied by the basilar artery, or at the borderzone areas, which are by definition the brain regions with the longest delay times. The easiest solution to this problem would be to implement any of the existing schemes to clearly define the bolus width and transit time, such as QUIPSS II (22), or rather Q2-TIPS (23), by repeatedly applying a parallel saturation slab around 2 cm proximally to the lowest acquired slice in both control and labeled scans. By carefully timing the signal detection after the saturation pulses, transit-time-insensitive perfusion images can in principle be acquired. Furthermore, the use of saturation pulses in both labeled and control acquisitions should reduce the artifactually high perfusion-like signal coming from remaining labeled intravascular spins, especially at the long inversion times used in this study. Although not flagrant in healthy volunteers, these effects of variable delay times between perfusion territories and the related remaining intravascular signal will become very important in patients. And then, even such schemes cannot account for the arrival time difference due to occlusion or other vascular disruptions, which are very frequent in the patient population targeted by the present method. Therefore, the combination of this method with a multislice turbo-readout, such as that presented in Ref. (24), might in such cases be more adequate, as it would provide measurements of both arrival time and perfusion separately.

In conclusion, we proposed in this work a new implementation of the RPI technique suitable for high field imaging, which can provide complete supratentorial coverage in either a shorter scan time (3 min/perfusion territory instead of 5 min) or higher resolution (80 × 80 instead of 64 × 64) than what can be reached at 1.5 T. It is therefore a first step toward a quantitative regional perfusion imaging technique; however, more work needs to be done on the absolute quantification and reproducibility of these measurements.

REFERENCES

1. Zhang W, Silva AC, Williams DS, Koretsky AP. NMR measurement of perfusion using arterial spin labeling without saturation of macromolecular spins. Magn Reson Med 1995;33:370–376.
2. Zaharchuk G, Ledden PJ, Kwong KK, Reese TG, Rosen BR, Wald LL. Multislice perfusion and perfusion territory imaging in humans with separate label and image coils. Magn Reson Med 1999;41:1093–1098.

3. Eastwood JD, Holder CA, Hudgins PA, Song AW. Magnetic resonance imaging with lateralized arterial spin labeling. Magn Reson Imaging 2002;20:583−586.

4. Hendrikse J, van der Grond J, Lu H, van Zijl PC, Golay X. Flow territory mapping of the cerebral arteries with regional perfusion MRI. Stroke 2004;35:882−887.

5. Davies NP, Jezzard P. Selective arterial spin labeling (SASL): perfusion territory mapping of selected feeding arteries tagged using two-dimensional radiofrequency pulses. Magn Reson Med 2003;49:1133−1142.

6. Edelman RR, Mattle HP, O'Reilly GV, Wentz KU, Liu C, Zhao B. Magnetic resonance imaging of flow dynamics in the circle of Willis. Stroke 1990;21:56−65.

7. Trampel R, Mildner T, Goerke U, Schaefer A, Driesel W, Norris DG. Continuous arterial spin labeling using a local magnetic field gradient coil. Magn Reson Med 2002;48:543−546.

8. Mildner T, Trampel R, Moller HE, Schafer A, Wiggins CJ, Norris DG. Functional perfusion imaging using continuous arterial spin labeling with separate labeling and imaging coils at 3 T. Magn Reson Med 2003;49:791−795.

9. Calamante F, Williams SR, van Bruggen N, Kwong KK, Turner R. A model for quantification of perfusion in pulsed labelling techniques. NMR Biomed 1996;9:79−83.

10. Golay X, Stuber M, Pruessmann KP, Meier D, Boesiger P. Transfer insensitive labeling technique (TILT): application to multislice functional perfusion imaging. J Magn Reson Imaging 1999;9:454−461.

11. Pruessmann KP, Golay X, Stuber M, Scheidegger MB, Boesiger P. RF pulse concatenation for spatially selective inversion. J Magn Reson 2000;146:58−65.

12. Lu H, Clingman C, Golay X, van Zijl PC. Determining the longitudinal relaxation time (T_1) of blood at 3.0 Tesla. Magn Reson Med 2004;52:679-682.

13. Frahm J, Bruhn H, Gyngell ML, Merboldt KD, Hanicke W, Sauter R. Localized high-resolution proton NMR spectroscopy using stimulated echoes: initial applications to human brain in vivo. Magn Reson Med 1989;9:79−93.

14. Edelman RR, Chen Q. EPISTAR MRI: multislice mapping of cerebral blood flow. Magn Reson Med 1998;40:800−805.

15. Ogg RJ, Kingsley PB, Taylor JS. WET, a T1- and B1-insensitive water-suppression method for in vivo localized 1H NMR spectroscopy. J Magn Reson B 1994;104:1−10.

16. Yongbi MN, Branch CA, Helpern JA. Perfusion imaging using FOCI RF pulses. Magn Reson Med 1998;40:938−943.

17. Nelder JA, Mead R. A simplex method for function minimization. Comput J 1965;7:308−313.

18. Bottomley PA, Hardy CJ, Argersinger RE, Allen-Moore G. A review of 1H nuclear magnetic resonance relaxation in pathology: are T1 and T2 diagnostic?. Med Phys 1987;14:1−37.

19. Oguz KK, Golay X, Pizzini FB, Freer CA, Winrow N, Ichord R, Casella JF, van Zijl PC, Melhem ER. Sickle cell disease: continuous arterial spin-labeling perfusion MR imaging in children. Radiology 2003;227:567−574.

20. Alsop DC, Detre JA. Multisection cerebral blood flow MR imaging with continuous arterial spin labeling. Radiology 1998;208:410−416.

21. Buxton RB, Frank LR, Wong EC, Siewert B, Warach S, Edelman RR. A general kinetic model for quantitative perfusion imaging with arterial spin labeling. Magn Reson Med 1998;40:383−396.

22. Wong EC, Buxton RB, Frank LR. Quantitative imaging of perfusion using a single subtraction (QUIPSS and QUIPSS II). Magn Reson Med 1998;39:702−708.

23. Luh WM, Wong EC, Bandettini PA, Hyde JS. QUIPSS II with thin-slice TI1 periodic saturation: a method for improving accuracy of quantitative perfusion imaging using pulsed arterial spin labeling. Magn Reson Med 1999;41:1246−1254.

24. Hendrikse J, Lu H, van der Grond J, Van Zijl PC, Golay X. Measurements of cerebral perfusion and arterial hemodynamics during visual stimulation using TURBO-TILT. Magn Reson Med 2003;50:429−433.